



Crystallization *via* tubing microfluidics permits both *in situ* and *ex situ* X-ray diffraction

Charline J. J. Gerard,^a Gilles Ferry,^b Laurent M. Vuillard,^b Jean A. Boutin,^b Leonard M. G. Chavas,^c Tiphaine Huet,^c Nathalie Ferte,^a Romain Grossier,^a Nadine Candoni^a and Stéphane Veesler^{a*}

Received 26 July 2017

Accepted 25 September 2017

Edited by L. J. Beamer, University of Missouri, USA

Keywords: crystallization; microfluidics; optimization; *in situ* X-ray diffraction; *ex situ* X-ray diffraction.

Supporting information: this article has supporting information at journals.iucr.org/f

^aCINaM–CNRS, Aix-Marseille Université, Campus de Luminy, Case 913, 13288 Marseille CEDEX 09, France, ^bInstitut de Recherches Servier, 125 Chemin de Ronde, 78290 Croissy-sur-Seine, France, and ^cPROXIMA-1, Synchrotron SOLEIL, Gif-sur-Yvette, France. *Correspondence e-mail: veesler@cinam.univ-mrs.fr

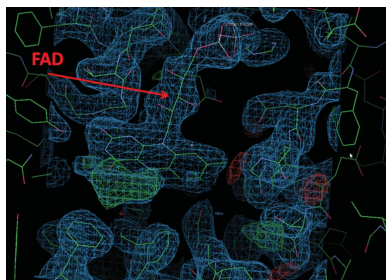
A microfluidic platform was used to address the problems of obtaining diffraction-quality crystals and crystal handling during transfer to the X-ray diffractometer. Crystallization conditions of a protein of pharmaceutical interest were optimized and X-ray data were collected both *in situ* and *ex situ*.

1. Introduction

Structural biologists need to solve three-dimensional structures of biological macromolecules *via* X-ray crystallography. Two decisive and rate-limiting steps are obtaining diffraction-quality crystals and handling crystals during transfer to the diffractometer.

Obtaining diffraction-quality crystals is complex and is influenced by many parameters (pH, temperature, types of buffer, salts and crystallization agents). Problems in producing suitable crystals can be tackled in two steps: (i) screening for favourable crystallization conditions in the phase diagram and (ii) optimizing crystal growth by developing a specific kinetic path in the phase diagram. Screening is an expensive task, both in terms of time and raw materials. Moreover, when only small quantities of sample materials are available, a suitable experimental tool is essential. Microfluidic techniques, *i.e.* the control and manipulation of flows on the submillimetre scale using a miniaturized device called a lab-on-a-chip (LOC; van der Woerd *et al.*, 2003), are appropriate for automating, miniaturizing and high-throughput crystallization approaches involving multiple operations such as mixing, analysis and separation (Leng & Salmon, 2009). LOCs are applied in both fast-screening and optimization stages of protein crystallization studies *via* the integration of traditional protocols of protein crystallization (Candoni *et al.*, 2012). Furthermore, the microfluidics approach suits the stochastic nature of nucleation (Hammadi *et al.*, 2015) because it allows multiple independent experiments.

Manual handling of the sample crystals can mechanically and environmentally stress them. The stress induced during this delicate step may affect the quality of the crystal and decrease its diffractive power. To minimize manual handling, an alternative is *in situ* X-ray data collection. One approach involves using X-ray-transparent microfluidic devices (Hansen *et al.*, 2006; Dhouib *et al.*, 2009; Stojanoff *et al.*, 2011; Guha *et al.*, 2012; Pinker *et al.*, 2013; Khvostichenko *et al.*, 2014; Horstman *et al.*, 2015; Heymann *et al.*, 2014; Maeki *et al.*, 2015).



© 2017 International Union of Crystallography

Another solution, following the pioneering work of Yadav *et al.* (2005), is to collect X-ray data directly in a microcapillary (Li *et al.*, 2006; Maeki *et al.*, 2012). For *ex situ* data collection, Gerdts *et al.* (2010) and Stojanoff *et al.* (2011) harvested a protein crystal from a microfluidic channel using a cryoloop and Li *et al.* (2006) made crystals flow out of a capillary and then looped and flash-cooled them.

We present an application that addresses these two problems using a microfluidic platform developed in our group (Zhang *et al.*, 2017). We apply our platform to the crystallization of a protein of pharmaceutical interest, human quinone reductase 2 (QR2; EC 1.10.5.1), which is involved in Alzheimer's disease (Hashimoto & Nakai, 2011), Parkinson's disease (Fu *et al.*, 2008) and oxidative stress (Nosjean *et al.*, 2000). We optimized the crystallization conditions of QR2 and collected X-ray data both *in situ* and *ex situ* to characterize the crystals obtained.

2. Optimization and crystallization results using the microfluidic platform

The microfluidic platform developed in our group offers four modular functions (Zhang *et al.*, 2017): droplet formation, online UV characterization, incubation and observation (Fig. 1). The microfluidic device is built using commercially available PEEK junctions and Teflon tubing, which were initially designed for high-performance liquid-chromatography systems, thus rendering it compatible with all solvents, simple, cheap, flexible and easily incorporated into any laboratory. We adapt the platform to generate droplets of 2 nl in long Teflon tubing (150 μm inner diameter; IDEX Health and Science) without using surfactant (Zhang *et al.*, 2015). Droplets are generated by crossing a continuous phase (FC70 fluorinated

oil from Hampton Research) with dispersed phases [containing the protein and the crystallization agent(s)] in a microfluidic junction (Te, cross or seven-entry junction from IDEX Health and Science according to the experimental requirements). A programmable syringe pump (neMESYS, Cetoni GmbH) controls the flow rates of the different fluids. We couple an online UV detector (USB2000+, Ocean Optics) to the Teflon tubing after the droplet-formation zone [labelled (3) in Fig. 1] using a home-made and specially designed UV cell (Zhang *et al.*, 2017). The tubing-wall material is sufficiently transparent under UV light. Thus, *in situ* spectral analysis of droplets is possible, allowing real-time acquisition; absorbance at one or several wavelengths can be recorded. Hence, the evolution of the chemical composition gradient in a group of generated droplets with identical size can be analyzed using the Beer–Lambert law.

Experimental conditions are based both on solubilities obtained by equilibrating crystal-solution suspensions over time (Fig. 1, Supporting Information) and the crystallization conditions used for structural determination (Foster *et al.*, 1999). Subsequent gradient optimization, using experimental conditions presented in Fig. 2, provides optimal conditions leading to high-quality crystals. At least 60 droplets of 2 nl per experimental condition were generated and observed (Fig. 2). The crystals in the droplets from experiment (b) in Fig. 2 were used for X-ray diffraction (XRD).

3. XRD characterization

Although direct X-ray data collection from the microfluidic devices is used to minimize manual handling, Teflon-related background noise is significant in the diffraction patterns. This may reduce the quality of the diffraction data (Yadav *et al.*,

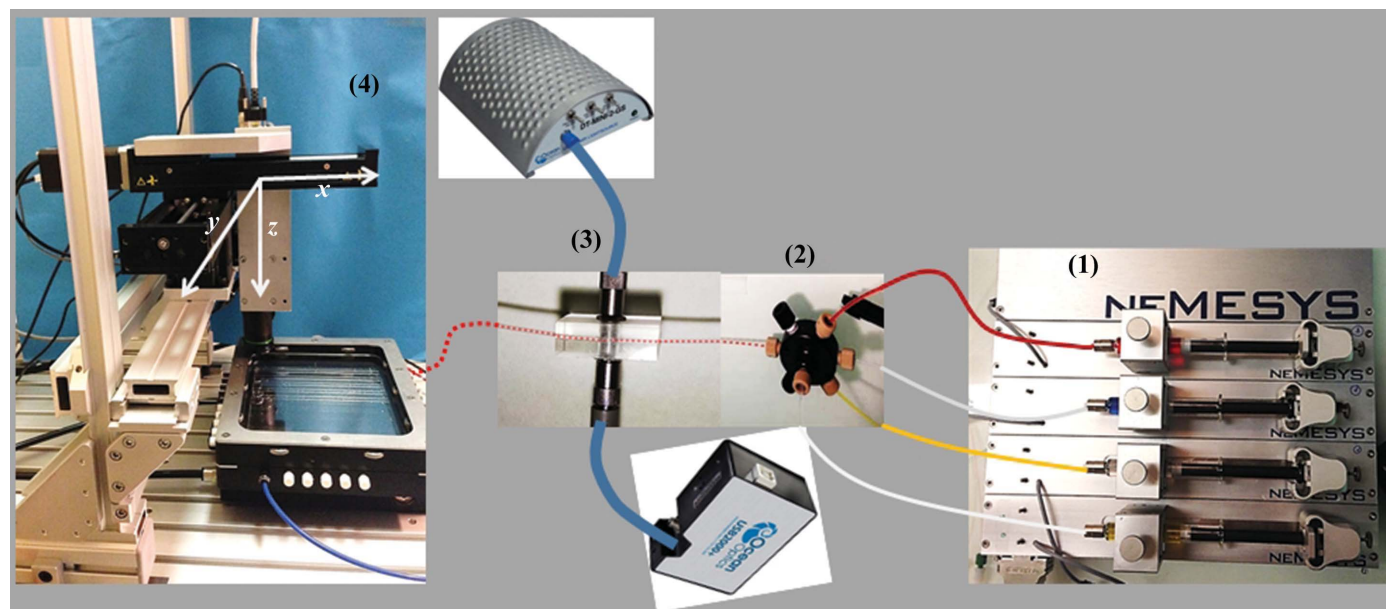


Figure 1
Pictures of the home-made microfluidic platform: (1) syringe pump, (2) seven-entry junction, (3) online UV module, (4) tubing holder for thermostating and observation with an XYZ-motorized camera.

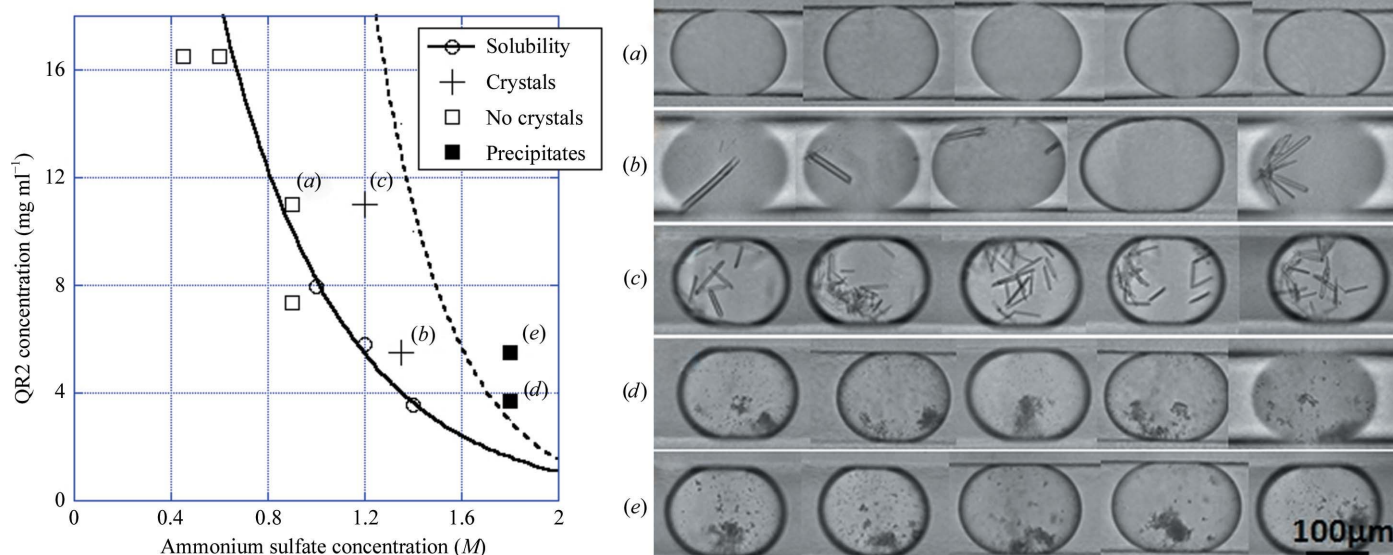


Figure 2 Left, solubility of QR2 versus ammonium sulfate at pH 8 (20 mM Tris-HCl, 150 mM NaCl; error bars are indicated by the size of the markers) and the different experimental conditions tested in the fine-gradient experiment. The dashed line is a guide for the eye to separate the crystallization and precipitation zones. Right, photographs of five representative droplets obtained as 2 nl droplets in a Teflon capillary (150 μm inner diameter) after 24 h. (a) 11 mg ml⁻¹ QR2, 0.9 M ammonium sulfate, (b) 5.5 mg ml⁻¹ QR2, 1.35 M ammonium sulfate, (c) 11 mg ml⁻¹ QR2, 1.2 M ammonium sulfate, (d) 3.7 mg ml⁻¹ QR2, 1.8 M ammonium sulfate, (e) 5.5 mg ml⁻¹ QR2, 1.8 M ammonium sulfate at 20°C.

2005) and strongly reduce the observed diffraction limits of the crystals. Hence, we tested two approaches: (i) transferring droplets containing the crystals of interest from Teflon to silica tubing for *in situ* XRD without cooling and (ii) extracting the crystals of interest from the tubing and depositing them on a MicroMesh, a polyimide grid transparent to X-rays, for *ex situ* XRD, thus avoiding mechanical shocks.

3.1. *In situ* XRD

We transferred the droplets from experiment (b) in Fig. 2, performed in Teflon tubing, to silica tubing (fused silica tubing with a polyimide coating of 150 μm inner diameter and 360 μm outer diameter; IDEX Health and Science) using a linear junction (IDEX Health and Science). The internal silica tubing wall was coated with a commercial hydrophobic surface-coating agent (Aqualpel, PPG Industry; Mazutis *et al.*,

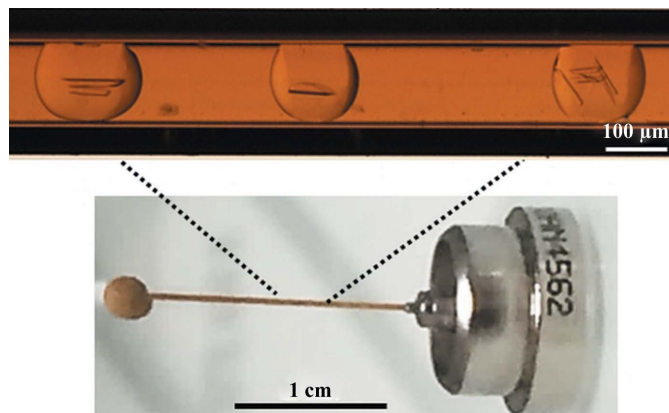


Figure 3 Photographs of the silica tubing mounted on a magnetic base.

2009) to ensure droplet stability. The silica tubing containing the droplets was directly mounted on a magnetic base extracted from standard SPINE sample loops, ready for transfer to the X-ray setup (Fig. 3). For a proof of concept, a single crystal was analysed by XRD at room temperature on the PROXIMA-1 beamline at Synchrotron SOLEIL. Diffraction was observed to a resolution of 2.7 Å (Fig. 2, Supporting Information). Ten images were taken at room temperature with 0.1 s exposure each before crystal deterioration. These diffraction data allowed us to determine the space group of the crystal, $P2_12_12_1$, and the unit-cell parameters ($a = 57.33$, $b = 83.03$, $c = 106.87$ Å). When XRD is carried out under cryogenic conditions, the same space group is described for the QR2 crystals and the unit-cell parameters are $a = 56.61$, $b = 83.16$, $c = 106.23$ Å, in accordance with the literature (Foster *et al.*, 1999). The strong X-ray damage to the crystal from these room-temperature measurements most likely explains why a complete data set could not be obtained from one single crystal.

Microfluidics, however, can produce hundreds to thousands of droplets with identical composition. Thus, serial crystallography at room temperature would yield a complete set of data for structural resolution with limited noticeable effects from radiation damage. This approach was used recently by Heymann *et al.* (2014) with a chip made of PDMS and COC (cyclic olefin polymer) or Kapton.

3.2. *Ex situ* XRD

Here, crystals were harvested from the Teflon tubing containing droplets. A droplet was deposited on a MicroMesh (MiTeGen) using a high-precision micro-injector for flow control (Elveflow). The micro-injector and the MicroMesh are

Table 1

Data-collection statistics.

Values in parentheses are for the highest resolution shell.

346	Diffraction source	PROXIMA-1, SOLEIL
347	Wavelength (Å)	0.97857
348	Temperature (K)	100
349	Detector	Dectris PILATUS 6M
350	Crystal-to-detector distance (mm)	440.50
351	Rotation range per image (°)	0.1
352	Total rotation range (°)	180
353	Exposure time per image (s)	0.1
354	Space group	$P2_12_12_1$
355	Unit-cell parameters (Å, °)	$a = 53.15, b = 81.62, c = 106.03,$ $\alpha = \beta = \gamma = 90$
356	Resolution (Å)	47.52–2.31 (2.37–2.31)
357	R_{merge} (%)	10.5 (68.7)
358	Completeness (%)	99.4 (93.8)
359	Total No. of reflections	87394
360	No. of unique reflections	20712 (1399)
361	Multiplicity	4.2 (3.9)
362	$\langle I/\sigma(I) \rangle$	8.0 (1.7)
363	Overall B factor from Wilson plot (Å ²)	26.99
364	$CC_{1/2}$	0.996 (0.687)

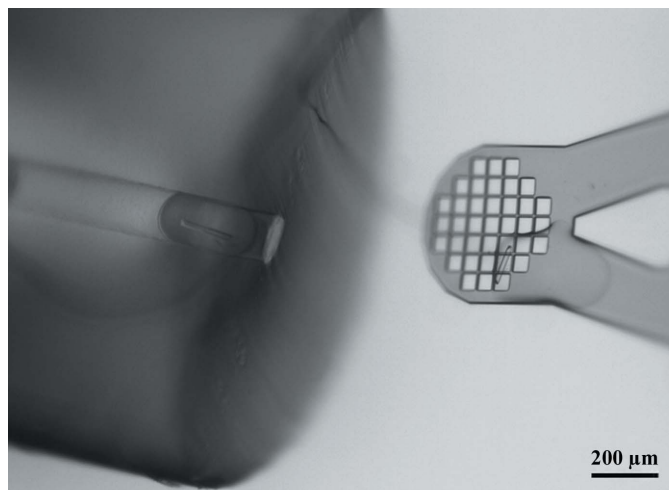


Figure 4

Photograph of a crystal in a droplet deposited on the MicroMesh.

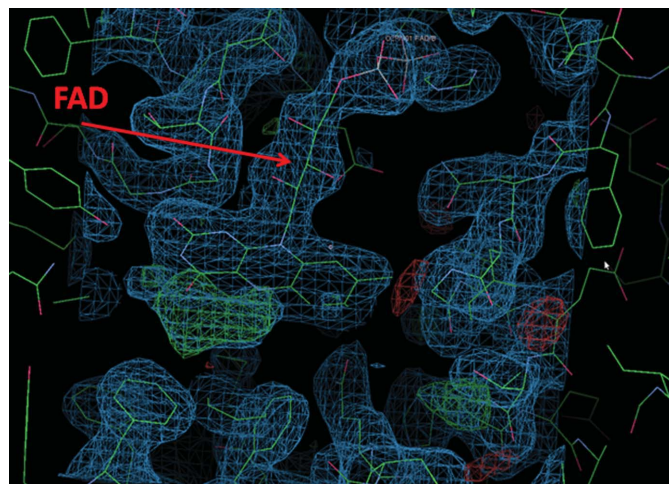


Figure 5

Electron-density map of the active site of QR2 with the FAD cofactor.

fixed to home-made micromanipulators for precise displacement in X , Y and Z (Grossier *et al.*, 2011; Fig. 3; Supporting Information). Crystals were placed singly on the MicroMesh (Fig. 4, Supplementary Fig. S4 and Supplementary Video S1), which was immediately extracted from the oil bath (FC70) and immersed in liquid nitrogen to cryogenize the crystals. Here the FC70 oil acted as a cryoprotectant, but crystals can be immersed in a drop of glycerol for cryoprotection. XRD was then carried out (Table 1). By extracting the crystals without direct handling or mechanical stress and preparing the sample for diffraction studies under cryogenic conditions, we were able to collect a full data set at a resolution of 2.3 Å (with or without glycerol). By determining the structure from one single crystal, we identified electron density for the flavin adenine dinucleotide (FAD) cofactor in the active site of QR2 (Fig. 5). Further studies should explore the screening of QR2 co-crystallization with ligands for structure-based drug design. These initial results confirm that the microfluidic approach yields crystallographic data of sufficient quality to allow us to judge whether or not the ligands bind to the active site.

4. Conclusions

We present the application of a microfluidic platform developed in our group to the optimization of the crystallization conditions for the pharmaceutical protein QR2. The resulting crystals were characterized by both *in situ* and *ex situ* X-ray diffraction.

5. Related literature

The following references are cited in the Supporting Information for this article: Gasteiger *et al.* (2003) and Veesler *et al.* (2004).

Acknowledgements

We thank the Institut de Recherche Servier for financial support. We thank T. Bactivelane (CINaM), M. Lagaize (CINaM) and M. Audiffren (ANACRISMAT) for technical assistance. We thank G. Sulzenbacher, S. Spinelli and P. Cantau (AFMB) for the transport of the crystals and their support with respect to crystallography. Experiments at Synchrotron SOLEIL were performed under in-house proposal No. 99150097.

Funding information

Results incorporated in this publication received funding from the European Union's Horizon 2020 research and innovation programme under grant agreement No. 708130.

References

- Candoni, N., Grossier, R., Hammadi, Z., Morin, R. & Veesler, S. (2012). *Protein Pept. Lett.* **19**, 714–724.
 Dhoub, K., Khan Malek, C., Pfleging, W., Gauthier-Manuel, B., Duffait, R., Thuillier, G., Ferrigno, R., Jacquamet, L., Ohana, J.,

457 Ferrer, J.-L., Théobald-Dietrich, A., Giegé, R., Lorber, B. & Sauter, C. (2009). *Lab Chip*, **9**, 1412–1421. 514

458 Foster, C. E., Bianchet, M. A., Talalay, P., Zhao, Q. & Amzel, L. M. (1999). *Biochemistry*, **38**, 9881–9886. 515

459 Fu, Y., Buryanovskyy, L. & Zhang, Z. (2008). *J. Biol. Chem.* **283**, 23829–23835. 516

460 Gasteiger, E., Gattiker, A., Hoogland, C., Ivanyi, I., Appel, R. D. & Bairoch, A. (2003). *Nucleic Acids Res.* **31**, 3784–3788. 517

461 Gerdts, C. J., Stahl, G. L., Napuli, A., Staker, B., Abendroth, J., Edwards, T. E., Myler, P., Van Voorhis, W., Nollert, P. & Stewart, L. J. (2010). *J. Appl. Cryst.* **43**, 1078–1083. 518

462 Grossier, R., Hammadi, Z., Morin, R., Magnaldo, A. & Veessler, S. (2011). *Appl. Phys. Lett.* **98**, 091916. 519

463 Guha, S., Perry, S. L., Pawate, A. S. & Kenis, P. J. A. (2012). *Sens. Actuators B Chem.* **174**, 1–9. 520

464 Hammadi, Z., Grossier, R., Zhang, S., Ikni, A., Candoni, N., Morin, R. & Veessler, S. (2015). *Faraday Discuss.* **179**, 489–501. 521

465 Hansen, C. L., Classen, S., Berger, J. M. & Quake, S. R. (2006). *J. Am. Chem. Soc.* **128**, 3142–3143. 522

466 Hashimoto, T. & Nakai, M. (2011). *Neurosci. Lett.* **502**, 10–12. 523

467 Heymann, M., Opathalage, A., Wierman, J. L., Akella, S., Szebenyi, D. M. E., Gruner, S. M. & Fraden, S. (2014). *IUCrJ*, **1**, 349–360. 524

468 Horstman, E. M., Goyal, S., Pawate, A., Lee, G., Zhang, G. G. Z., Gong, Y. & Kenis, P. J. A. (2015). *Cryst. Growth Des.* **15**, 1201–1209. 525

469 Khvostichenko, D. S., Schieferstein, J. M., Pawate, A. S., Laible, P. D. & Kenis, P. J. A. (2014). *Cryst. Growth Des.* **14**, 4886–4890. 526

470 Leng, J. & Salmon, J. B. (2009). *Lab Chip*, **9**, 24–34. 527

471 Li, L., Mustafi, D., Fu, Q., Tereshko, V., Chen, D. L., Tice, J. D. & Ismagilov, R. F. (2006). *Proc. Natl Acad. Sci. USA*, **103**, 19243–19248. 528

472 Maeki, M., Pawate, A. S., Yamashita, K., Kawamoto, M., Tokeshi, M., Kenis, P. J. A. & Miyazaki, M. (2015). *Anal. Chem.* **87**, 4194–4200. 529

473 Maeki, M., Yoshizuka, S., Yamaguchi, H., Kawamoto, M., Yamashita, K., Nakamura, H., Miyazaki, M. & Maeda, H. (2012). *Anal. Sci.* **28**, 65. 530

474 Mazutis, L., Araghi, A. F., Miller, O. J., Baret, J.-C., Frenz, L., Janoshazi, A., Taly, V., Miller, B. J., Hutchison, J. B., Link, D., Griffiths, A. D. & Ryckelynck, M. (2009). *Anal. Chem.* **81**, 4813–4821. 531

475 Nosjean, O., Ferro, M., Cogé, F., Beauverger, P., Henlin, J.-M., Lefoulon, F., Fauchère, J.-L., Delagrangé, P., Canet, E. & Boutin, J. A. (2000). *J. Biol. Chem.* **275**, 31311–31317. 532

476 Pinker, F., Brun, M., Morin, P., Deman, A.-L., Chateaux, J.-F., Oliéric, V., Stirnimann, C., Lorber, B., Terrier, N., Ferrigno, R. & Sauter, C. (2013). *Cryst. Growth Des.* **13**, 3333–3340. 533

477 Stojanoff, V., Jakoncic, J., Oren, D. A., Nagarajan, V., Navarro Poulsen, J.-C., Adams-Cioaba, M. A., Bergfors, T. & Sommer, M. O. A. (2011). *Acta Cryst.* **F67**, 971–975. 534

478 Veessler, S., Fertè, N., Costes, M.-S., Czjzek, M. & Astier, J.-P. (2004). *Cryst. Growth Des.* **4**, 1137–1141. 535

479 Woerd, M. van der, Ferree, D. & Pusey, M. (2003). *J. Struct. Biol.* **142**, 180–187. 536

480 Yadav, M. K., Gerdts, C. J., Sanishvili, R., Smith, W. W., Roach, L. S., Ismagilov, R. F., Kuhn, P. & Stevens, R. C. (2005). *J. Appl. Cryst.* **38**, 900–905. 537

481 Zhang, S., Fertè, N., Candoni, N. & Veessler, S. (2015). *Org. Process Res. Dev.* **19**, 1837–1841. 538

482 Zhang, S., Gerard, C. J. J., Ikni, A., Ferry, G., Vuillard, L. M., Boutin, J. A., Ferte, N., Grossier, R., Candoni, N. & Veessler, S. (2017). *J. Cryst. Growth*, **472**, 18–28. 539

483 540

484 541

485 542

486 543

487 544

488 545

489 546

490 547

491 548

492 549

493 550

494 551

495 552

496 553

497 554

498 555

499 556

500 557

501 558

502 559

503 560

504 561

505 562

506 563

507 564

508 565

509 566

510 567

511 568

512 569

513 570